Increasing temporal resolution of DSC perfusion MRI using the analytic image concept

Yankam Njiwa, J ; Ratering, D ; Baltes, C ; Rudin, M

Abstract: OBJECT: Dynamic susceptibility contrast MRI (DSC-MRI) is increasingly being used to evaluate cerebral microcirculation. In this study, the use of the analytic image reconstruction (AIR), with the aim to increase the temporal resolution, is evaluated for DSC-MRI in small animals. MATERIALS AND METHODS: Imaging was performed using a T (2)*- weighted sequence to acquire male Lewis rats raw data. Results show that AIR satisfactory reconstructs DSC-MRI while preserving a good reconstruction quality and the image characteristics compared to the full k-space and keyhole reconstructed images. The combination of the choice of the baseline image and the proposed asymmetric acquisition schema enables an increase in temporal resolution, by a factor of four, thus having more sample points for better estimating perfusion parameters. RESULTS: Computer simulations result in a mean cerebral blood volume of 1.22 that deviates from the full k-space value by -3% and a mean cerebral blood flow of 1.97 deviating from the full k-space value by -3% when the mean transit time did not change. Even if these deviations increase when achieving real acquisitions, AIR still better computes quantitative values than keyhole. CONCLUSION: AIR allows a good reconstruction of the dynamic stage of the image series thus leading to better dynamic effects analysis.

DOI: https://doi.org/10.1007/s10334-010-0224-9

Magn Reson Mater Phy (2010) 23:251–261
DOI 10.1007/s10334-010-0224-9

RESEARCH ARTICLE

Increasing temporal resolution of DSC perfusion MRI using the analytic image concept

Josiane Yankam Njiwa · David Ratering · Christof Baltes · Markus Rudin

Received: 13 April 2010 / Revised: 7 July 2010 / Accepted: 19 July 2010 / Published online: 7 August 2010

Abstract
Object Dynamic susceptibility contrast MRI (DSC-MRI) is increasingly being used to evaluate cerebral microcirculation. In this study, the use of the analytic image reconstruction (AIR), with the aim to increase the temporal resolution, is evaluated for DSC-MRI in small animals.
Materials and methods Imaging was performed using a T_2*- weighted sequence to acquire male Lewis rats raw data. Results show that AIR satisfactory reconstructs DSC-MRI while preserving a good reconstruction quality and the image characteristics compared to the full *k*-space and keyhole reconstructed images. The combination of the choice of the baseline image and the proposed asymmetric acquisition schema enables an increase in temporal resolution, by a factor of four, thus having more sample points for better estimating perfusion parameters.
Results Computer simulations result in a mean cerebral blood volume of 1.22 that deviates from the full *k*-space value by −3% and a mean cerebral blood flow of 1.97 deviating from the full *k*-space value by −3% when the mean transit time did not change. Even if these deviations increase when achieving real acquisitions, AIR still better computes quantitative values than keyhole.
Conclusion AIR allows a good reconstruction of the dynamic stage of the image series thus leading to better dynamic effects analysis.

Keywords Acquisition time · Dynamic susceptibility MRI · Analytic image · Partial *k*-space reconstruction · MRI

J. Yankam Njiwa · D. Ratering · C. Baltes · M. Rudin
Institute for Biomedical Engineering,
University and ETH Zurich, Zurich, Switzerland

M. Rudin
Institute of Pharmacology and Toxicology,
University of Zurich, Zurich, Switzerland

J. Yankam Njiwa (✉)
AIC-ETH, HIT E22, Wolfgang Pauli-Strasse 27,
8093 Zurich, Switzerland
e-mail: njiwa@biomed.ee.ethz.ch

Introduction

Brain perfusion is an important measure for the local supply of nutrients and oxygen to brain tissue. Magnetic resonance imaging (MRI) represents an ideal technology for assessing brain perfusion in a non-invasive and spatially resolved manner. When using tracer dilution methods, a contrast agent (CA) is administered intravenously and the first passage of this CA bolus through the brain is monitored using MRI. This dynamic susceptibility contrast MRI (DSC-MRI) technique yields hemodynamic parameters related to the cerebral blood flow (CBF), the cerebral blood volume (CBV) and the mean transit time (MTT) of the contrast agent. The fast passage of the CA puts high demands on the temporal resolution of the MR data collection, while reasonable spatial resolution should be maintained.

Several methods have been proposed to improve the efficiency of the data acquisition by reducing the amount of acquired data by so-called assuming that some prior information about the object is already known. Methods exploiting temporal redundancies include keyhole [1–6] and view-sharing methods [7–11].

In DSC-MRI, contrast arises from signal dephasing around vessels containing contrast agent in T_2^*-weighted images, which leads to a signal attenuation that is assumed to be proportional to the concentration of the contrast agent in the blood in absence of saturation effects. The keyhole

technique, where only the central region of the Fourier domain is acquired, improves temporal resolution while retaining Cartesian sampling. The basic prerequisite of keyhole imaging demands that the change in the dynamic series is of a nature that can be sufficiently covered by the central part of the Fourier domain. Thus, low spatial frequencies should be sufficient to describe the changes in the image series, implying that they are affecting coarse rather than fine structures [5]. The spatial resolution of the dynamic data is governed by the number of phase-encoding lines sampled in the keyhole segment, across the Fourier domain center, which by itself is determined by the condition that approximately 90% of the signal power in an image should be retained within this segment. Pitfalls of inappropriate positioning of the keyhole window include severe artifacts, such as bad estimation of perfusion parameters or wrong computation of T_2* map values, in the analysis of dynamic effects which are due to an erroneous time curve [5], loss of the signal behavior at each time point in the dynamic information and signal drifts in *k*-space that become especially prominent in T_2*-weighted DSC-MRI. Therefore, despite the advantage of improved temporal resolution, the keyhole technique is not widely used in a clinical setting.

To address the aforementioned limitations, such as signal drifts in *k*-space, erroneous time curve which leads to bad estimation of perfusion parameters, we have evaluated the capabilities of the analytic image reconstruction (AIR) technique [12], which also exploits redundancies in time in its reconstruction process, for reconstructing DSC-MRI raw data. The method is based on the principle of acquiring only the symmetric low-frequency part of the *k*-space data in order to reduce the acquisition time then to replace the missing high spatial frequencies as illustrated in Fig. 1c. For reconstruction, each dynamic *k*-space is split into two parts, the positive spatial frequencies covering half of *k*-space and the negative spatial frequencies covering only the central part of the other half of *k*-space. These two parts are considered as the spectral representations of two individual analytic images. The final image is then computed by taking the magnitude of the sum of these two reconstructed images. AIR has already been compared to partial Fourier reconstruction methods like homodyne detection [13] and projection onto convex sets (POCS) [14] for human dynamic imaging and was shown to yield superior results [15], mainly because there is no need to compensate for phase errors during image reconstruction in order to expect its good reconstruction quality. In the present work, we investigated the AIR approach for reconstructing DSC-MRI and studied its capabilities of reproducing perfusion measurements in small animal studies. For this purpose, AIR was compared both to full *k*-space and keyhole reconstructions.

Theoretical background

The analytic image concept has been described previously [12,15]; for reasons of clarity, we will illustrate the principles as far as they are required for reconstructing 2-D dynamic MR images.

Irrespective of the acquisition procedure and neglecting noise, a given full *k*-space data set $S(u, v)$ can be expressed as the superposition of its negative and positive spatial frequencies in the phase-encoding direction (u), i.e. $S(u, v) = S_n(u, v) + S_p(u, v)$. Inverse Fourier transformation of $S_{n,p}(u, v)$ yields the real images $f_{n,p}(x, y)$, with n and p standing for negative or positive. Due to magnetic field inhomogeneities and/or eddy currents effects, $S(u, v)$ is in general not Hermitian. Nevertheless, assuming deviations to be small, we can assume pseudo-Hermitian symmetry.

The analytic images $z_p(x, y)$ and $z_n(x, y)$ associated to the positive and the negative half *k*-space are defined as

$$z_{n,p}(x, y) = f_{n,p}(x, y) + \frac{j}{\pi} \cdot p.v. \int_{-\infty}^{+\infty} \frac{f_{n,p}(\tau, y)}{x - \tau} \cdot \mathrm{d}\tau, \tag{1}$$

where *p.v.* stands for the Cauchy principal value, and

$$f_{n,p}(x, y) = \mathrm{Re}\left[F_2^{-1}\left(S_{n,p}(u, v)\right)\right]$$

with

$$S_{n,p}(u, v) = (1 + \mathrm{sgn}(u)) \cdot F_2(f_{n,p})(u, v). \tag{2}$$

F_2 represents the 2-D Fourier transform operator. Finally, the analytic image $z(x, y)$ describing the full *k*-space is given by

$$z(x, y) = f_p(x, y) + f_n(x, y) + \frac{j}{\pi} \cdot p.v. \int_{-\infty}^{+\infty} \frac{f_p(\tau, y)}{x - \tau} \cdot \mathrm{d}\tau + \frac{j}{\pi} p.v. \int_{-\infty}^{+\infty} \frac{f_n(\tau, y)}{x - \tau} \cdot \mathrm{d}\tau. \tag{3}$$

In the following, we extend the analytic image concept to dynamic MR images and include the time t as additional variable. In this case, the full *k*-space $S(u, v, t)$ is partitioned into two parts $S_n(u, v, t)$ and $S_p(u, v, t)$ and Eq. 3 becomes

$$z(x, y, t) = f_p(x, y, t) + f_n(x, y, t) + \frac{j}{\pi} \cdot p.v. \int_{-\infty}^{+\infty} \frac{f_p(\tau, y, t)}{x - \tau} \cdot \mathrm{d}\tau + \frac{j}{\pi} \cdot p.v. \int_{-\infty}^{+\infty} \frac{f_n(\tau, y, t)}{x - \tau} \cdot \mathrm{d}\tau. \tag{4}$$

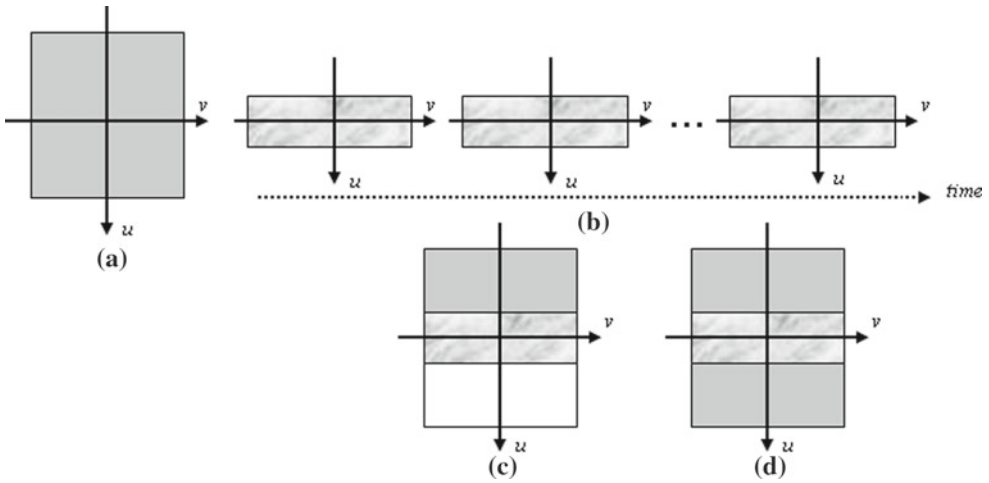

Fig. 1 *k*-space sampling strategies: **a** Baseline data set covering full *k*-space **b** Dynamic acquisition of symmetric low spatial frequencies in the phase-encoding direction of *k*-space (*k*-space center). Low spatial frequencies representing the dynamic data are merged with the baseline high spatial frequencies to form the optimal reconstruction data set for AIR (**c**) and keyhole reconstruction (**d**), respectively

We now assume the *k*-space to be sampled asymmetrically (Fig. 1c) comprising all the positive *k*-space frequencies together with few negative frequencies in the phase-encoding direction for any given time *t*. In this case, Eq. 4 can be rewritten as

$$z(x,y,t) = f_p(x,y,t) + f_n(x,y,t) + \frac{j}{\pi}\cdot p.v. \times \int_{-\infty}^{+\infty} \frac{f_p(\tau,y,t)}{x-\tau}\mathrm{d}\tau + \frac{j}{\pi}\cdot p.v. \int_{-\infty}^{+\infty} \frac{f_n(\tau,y,t)}{x-\tau}\cdot \mathrm{d}\tau \otimes \left(\frac{\delta(y)}{2} + \frac{1}{j\cdot 2\pi\cdot y}\right) \quad (5)$$

where the last term of the right side of Eq. 5 represents the inverse Fourier transform of a step function (the lower truncation frequency is $-N/8$, N being the total number of phase-encoding lines), and accounts for the fact that the negative *k*-space is only sampled in part. The final reconstructed image $f(x,y,t)$ is then obtained by computing the magnitude of $z(x,y,t)$.

Figure 2 schematically compares *k*-space sampling using AIR and keyhole strategies. For simplicity, we illustrate the 1-D case. The major difference when comparing AIR with keyhole reconstruction lies on the different weighting of the central *k*-space frequencies. Based on this, we also analyzed a modified keyhole reconstruction (m_keyhole), for which the low spatial frequencies were multiplied with a weight factor (2) to mimic the AIR, using the same amount of raw data.

Materials and methods

Animal preparation

In vivo experiments were carried out on male Lewis rats ($N = 10$) of 200–380 g body weight with unrestricted access to standard rat chow and tap water. Animals were anaesthetized using an initial dose of 4% isoflurane in an air/oxygen mixture (4:1), endotracheally intubated and artificially ventilated using a small animal ventilator (Maraltec, Biel-Benken, Switzerland). Anesthesia was maintained throughout the experiment using a dose of 1.5% isoflurane. Body temperature was monitored using a rectal temperature probe and maintained at 36.5 ± 0.5°C using warm air. The tail vein was cannulated for administration of the contrast agent. All experiments were carried out in strict adherence to the Swiss law for animal protection.

MRI experiments

MR experiments were carried out using a Bruker BioSpec 94/30 (Bruker BioSpin MRI, Ettlingen, Germany) small animal MR system operating at 400 MHz. A linear polarized volume resonator was used for excitation and a quadrature surface coil for signal reception. Positioning of the imaging slice for the perfusion measurements was planned on sagittal and coronal scout images. As we were also aiming to investigate the capabilities of AIR compared to keyhole for reconstructing dynamic phenomena, we choose to use a FLASH (fast low-angle shot) sequence instead of an EPI sequence (echo planar imaging: method of choice for DSC imaging), as the latter is more susceptible to image distortions and will probably make difficult comparison of

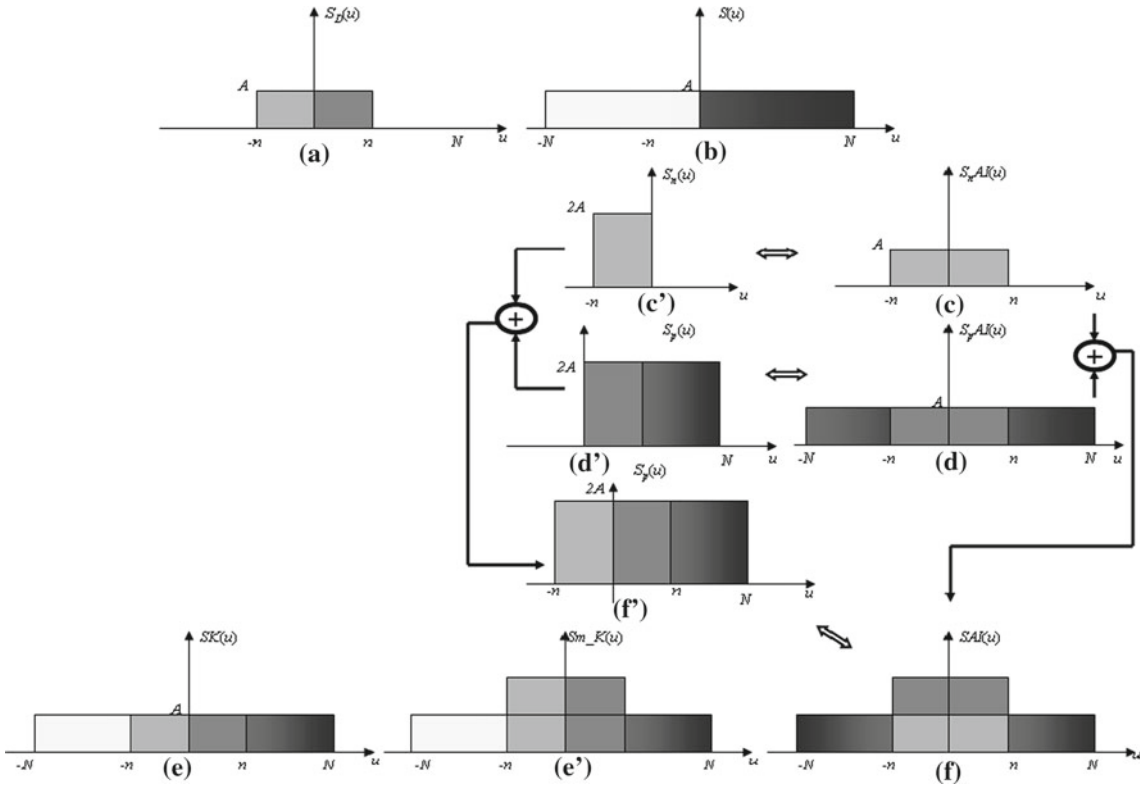

Fig. 2 Schematic description of AIR and keyhole reconstructions along the phase-encoding direction of *k*-space (in 1D for simplicity). Combining low resolution dynamically acquired data (**a**) and fully sampled baseline data (**b**). For AIR the original data are split into negative (**c'**) and positive (**d'**) frequencies, respectively, and complemented by complex conjugation to yield the spectral representations (**c**) and (**d**). Combination of (**c**) and (**d**) yields the dataset (**f**) used for the AIR image reconstruction. Substituting the low frequency part of (**b**) with (**a**) yields data set (**e**) used for keyhole reconstruction. Finally, multiplying the low frequency components in (**e**) with a factor 2 yields (**e'**) used for m_keyhole reconstruction

reconstruction results. In any case, the DSC-MRI action on the intravoxel magnetic field distribution is entirely independent from the imaging technique employed to detect it, therefore any suitable MRI sequence should yield similar results. AIR is expected to approach the time resolution of EPI imaging by reducing the number of phase-encoding lines acquired. For the estimation of brain perfusion, axial T_2^*-weighted images were acquired before, during and after contrast agent administration using a gradient echo sequence (FLASH) with the following parameters: slice thickness (STH) = 1.5 mm, field of view (FOV) = $26 \times 26\,\text{mm}^2$, matrix dimension (MD) = 400×55 for full *k*-space sampling and 400×15 when acquiring only the center part of *k*-space, reconstruction matrix (RM) = 512×55, flip angle (α) = 10°, echo time/repetition time (TE/TR) = 5/18.2 ms. For full *k*-space sampling, 128 repetitions, with a temporal resolution of 1 s, were acquired resulting in a total acquisition time of 128 s, while reduced *k*-space sampling resulted in an increased temporal resolution of 273 ms. Correspondingly, the number of repetitions was increased to 470 thereby maintaining the same total acquisition time of 128 s. The contrast agent Endorem® (Laboratoires Guerbet Sam Paris, France) was administered after 20 repetitions (injected volume: 0.5 ml, concentration: 11.2 mg Fe/ml, infusion rate: 0.5 ml/min) using an automatic injection pump (Havard Apparatus, PHD2000 series, Plymouth Meeting, USA). The pump was started and stopped by TTL pulses prompted by the MRI pulse program.

K-space sampling and image reconstruction

Prior to the acquisition of dynamic image series, a fully sampled baseline image was acquired as presented on Fig. 1a. Subsequently, series of fully sampled images were collected in five animals representing reference DSC measurements, while an image series with high temporal resolution, collecting only the central part of *k*-space, was acquired in another 5 animals (Fig. 1b).

During reconstruction, positive high spatial frequencies from the baseline *k*-space and low spatial frequencies from the dynamic image series were combined (Fig. 1c) and reconstructed to a high spatial and high temporal resolution image series using the analytic image concept. Accordingly,

keyhole reconstruction was performed by updating the low spatial frequencies of the baseline *k*-space with the central *k*-space lines acquired in the dynamic scan. Subsequently, each image series is reconstructed independently according to the obtained *k*-space. To allow for a direct comparison between AIR and keyhole, the central *k*-space lines were attributed twice the weight for a modified keyhole reconstruction (m_keyhole). The increased weighting of central *k*-space is inherent in AIR. The various reconstruction approaches were implemented in Matlab (R2007b, Math Works Inc., USA). In addition, the performance of AIR, keyhole and m_keyhole was compared using synthetic datasets. For this purpose, the number of phase-encoding lines of a fully sampled *k*-space data was reduced according to the sampling scheme described for AIR and keyhole (Fig. 1a, b) assuming different reduction factors (and correspondingly acquisition times) and images reconstructed using the respective algorithms.

Image analysis

Performance analysis

Qualitative assessment of the reconstructed images was performed by calculating the difference images between fully sampled images and images reconstructed from partial *k*-space acquisitions in combination with AIR, keyhole and m_keyhole reconstructions. Difference images were computed according to

$$\mathrm{DIFF} = |I(x, y) - I_R(x, y)| \tag{6}$$

where $I(x, y)$ is the full *k*-space reconstructed image taken as reference and $I_R(x, y)$ the AIR, keyhole or m_keyhole reconstructed image series. For quantitative evaluations, we used, as a first criterion, the normalized mean squared error (NMSE) defined by

$$\mathrm{NMSE} = \frac{1}{N}\sum\sum \frac{(I(x, y) - I_R(x, y))^2}{\bar{I}.\bar{I}_R}, \tag{7}$$

with $\bar{I}$ and $\bar{I}_R$ being the mean image intensities of $I(x, y)$ and $I_R(x, y)$, respectively.

The signal-to-noise ratio (SNR) was used as a second criterion for evaluating the reconstruction quality. For this purpose, one region of interest (ROI) was positioned in the rat cortex serving as signal estimate. The cortical SNR ($\mathrm{SNR}_{\mathrm{Cortex}}$) at maximum concentration was then computed, according to Liu [16], as

$$\mathrm{SNR}_{\mathrm{Cortex}} = C_{\max}/\sigma_{C\,\max} \tag{8}$$

where $C_{\max}$ is the maximum value of the concentration–time curve expressed in Eq. 10, and $\sigma_{C\,\max}$ is the noise variance of $C(t)$ when $C(t) = C_{\max}$.

Analysis of perfusion data

Quantitative analysis was carried out using the same cortical ROI as above. Signal intensity values over time $I(t)$ were converted to relative concentrations $C(t)$ of the CA according to

$$C(t) \propto -\frac{1}{\mathrm{TE}} \ln\left[I(t)/I(0)\right] \tag{9}$$

where $I(0)$ represents the intensity prior to CA administration and TE the echo time. It was assumed that cerebral blood volume (CBV) did not change during the measurements. To estimate the CBV, we first estimated an arterial input function (AIF) as described in Yeh et al. [17]. In our case, the AIF was obtained from 10 pixels with greatest contrast enhancement and relying on the work of Newman [18], cerebral blood volume was then computed by the parametric area under the curve (AUC) through the following formula

$$\mathrm{CBV} = \frac{h\int -\ln(I(t)/I(0))\mathrm{d}t}{\rho\int -\ln(I_a(t)/I_a(0))\mathrm{d}t} \tag{10}$$

where $I_a(0)$ and $I_a(t)$ are the arterial signal intensity prior to and at time t following the CA administration. h is a coefficient correcting for the differences in hematocrit between large vessels and the brain vasculature with a value of 0.73 being reported, and ρ standing for the attenuation of the brain tissue (1.04 g/ml) [20]. We used a non-parametric deconvolution model based on the Fourier transform as described by Ostergaard et al. [19] to compute the CBF value. The CBF is estimated from the maximum value of the deconvolved function. The mean transit time MTT is computed using the central volume theorem [21],

$$\mathrm{MTT} = \mathrm{CBV}/\mathrm{CBF}. \tag{12}$$

Results

Computer simulations

The performance of AIR was compared to images reconstructed from full *k*-space, keyhole and the m_keyhole sampling schemes. In order to achieve optimal correspondence of raw data, partial *k*-space data sets were generated from the full *k*-space sample setting the respective high frequency *k*-space lines to zero (see below). Images shown were recorded prior to the administration of the CA (Pre), during (Peak) and after (Post) the first pass of the CA, respectively. To construct the data set presented in Fig. 1d, the first image of the image series was fully sampled and used as baseline. For subsequent images, only 25% of the data around the center of *k*-space was kept. The missing high spatial frequencies of the *k*-space image series were updated using the high

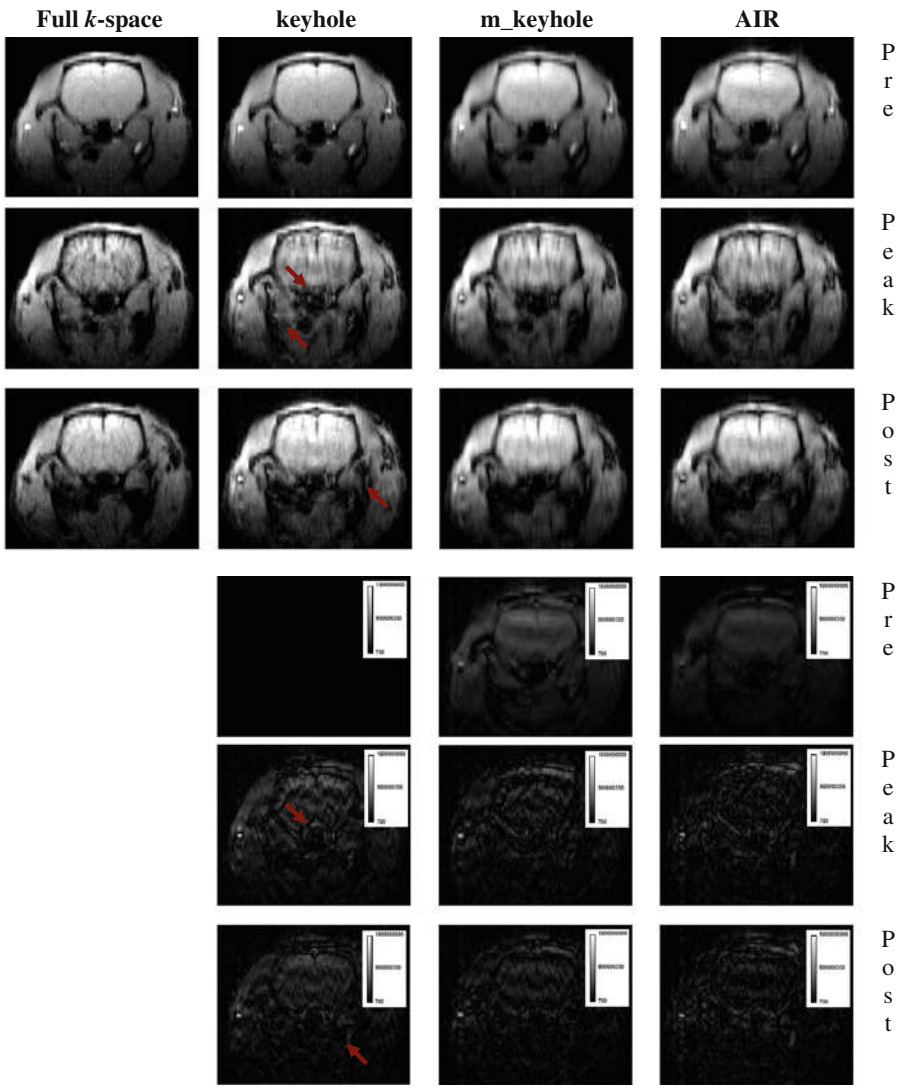

Fig. 3 Simulation results: Axial images of rat brain acquired previous (Pre), during (Peak) and after (Post) the CA passage. Left column are full *k*-space reconstructed images while the middle and right columns are images reconstructed with keyhole and AIR reconstruction methods, respectively. Simulation of reduced *k*-space acquisition is achieved using full raw data acquired on the same animal. 25% of the full *k*-space data are kept to perform keyhole and AIR reconstructions. Absolute difference images (DIFF) were compute between the full *k*-space reconstructed images and the partial *k*-space reconstructed ones before, during and after the first passage of the CA. In images, reconstructed using keyhole during and after the first pass of the CA artifacts have been observed that could be mistaken as anatomical structures (*arrows*)

frequencies of the baseline (Fig. 1). The comparison of images reconstructed from fully sampled *k*-space (Fig. 3, left column) with images from partial *k*-space sampling (using only 25% of *k*-space data corresponding to a reduction factor of 4) shows no obvious degradation in image quality for the keyhole reconstructed images prior to CA administration, while spatial blurring appeared in m_keyhole, AIR and keyhole images following CA administration. Qualitative inspection of the images revealed superior anatomical definition (edges, high-frequency structures) for keyhole when compared to AIR and m_keyhole reconstructions, especially before CA injection. On the other hand, quantitative analysis yielded significantly larger deviations of intensity for keyhole with regard to the other two techniques. These observations are consolidated by the error values plotted in Fig. 4. The NMSE in keyhole is consistently larger than that of AIR or m_keyhole especially after the CA injection. The changes in NMSE over time are due to the fact that the average image intensity changes upon passage of the CA (Eq. 8). Particularly, in keyhole, some misleading artifacts occur in the images reconstructed during and after the first pass of the CA (indicated by arrows in Fig. 3). As the number of phase-encoding lines kept for reconstructing the dynamic effects appears to be too small, keyhole images are dominated by features present in the baseline image.

The comparison of the NMSE reveals that the dynamic changes are better reconstructed using AIR compared to keyhole approach (Fig. 4). Furthermore, m_keyhole and AIR which are of comparable level lead to higher SNR values compared to conventional keyhole.

For quantitative evaluations of perfusion data, we analyzed the signal intensity profile for two ROIs, the first one located in the rat cerebral cortex and the second in the brain striatum, and computed the regional concentration–time curves (rCTC). The data points corresponding to the first pass of the rCTC (for both tissue and AIF) were used to

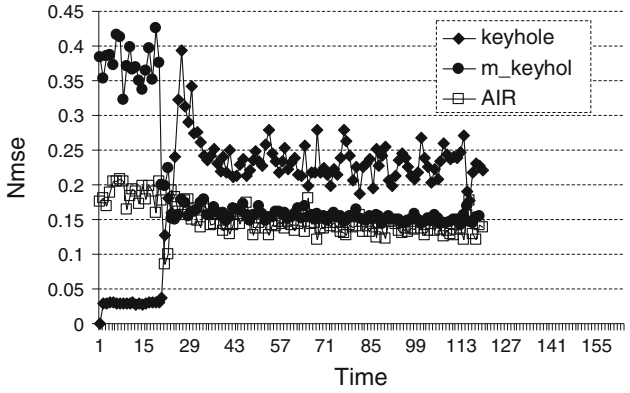

Fig. 4 Quantitative evaluation of perfusion images when simulating reduced *k*-space sampling: NMSE evolution during time. The acquired data represents 25% of the full *k*-space

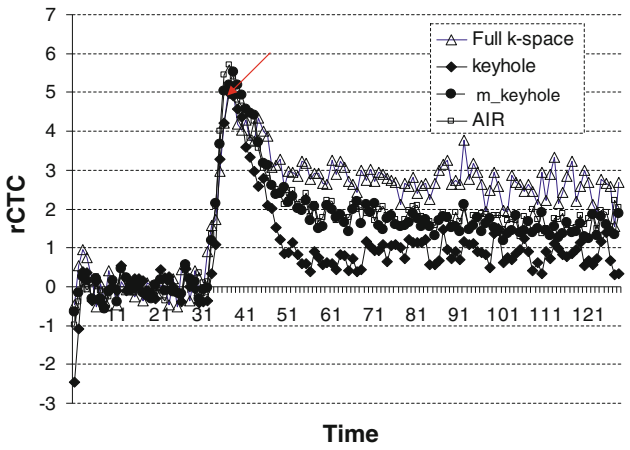

Fig. 5 Quantitative evaluation of simulated reduced perfusion data: Concentration–time curve (CTC) from full and reduced *k*-space reconstructions. The arrow indicates the peak of the keyhole CTC curve. 25% of the full *k*-space is used to perform AIR, keyhole and m_keyhole

compute perfusion parameters (see Materials and Methods). For comparison, rCTC values have been computed after re-scaling all the reconstructed images to the same range of intensities. The comparison of the rCTC curves of full *k*-space image series and partial *k*-space reconstruction, for a cortical ROI, using keyhole, m_keyhole and AIR approaches, using 25% of the full *k*-space data, is shown in Fig. 5 for one representative animal. Corresponding perfusion parameters (regional CBV, MTT and regional CBF) are listed in Table 1a for the brain cortex and in Table 1b for the brain striatum. Perfusion parameters computed for AIR images deviated of −3% for rCBV, 0% for MTT and −3% for rCBF, in the cortical ROI, when compared to the reference values computed for the full *k*-space reconstructed data, which is within one standard deviation of the reference values. The aforementioned parameters deviated of 3% for rCBV, 22% for MTT and −24% for rCBF, in the striatum. The corresponding values are significantly larger for m_keyhole and in particular for keyhole. The difference observed in terms of MTT values computation is probably due to the contribution of the high spatial frequencies in each considered ROI. That is also expressed by the computation of SNR values, for which a noticeable increase is observed in comparison to the full *k*-space reconstruction. The lack of half of the high spatial frequencies reduces the noise contribution in the reconstructed images (AIR). Figure 5 also shows that the recirculation property of the CA used, i.e. its steady-state concentration that is attained following tracer first pass, is poorly accounted for by the keyhole reconstruction.

Increase in temporal resolution in dynamic susceptibility contrast MRI

Five animals each were imaged to acquire full or reduced *k*-space data sets. Again, performances of AIR were compared to those of full *k*-space, keyhole and m_keyhole reconstructions using only 25% of *k*-space data corresponding to a reduction in the acquisition time by a factor of 4 (Fig. 6). The quality of images reconstructed on the basis of partial *k*-space datasets is considered satisfactory, even though keyhole displays some artifacts originating from the static part of the image. Images reconstructed with both keyhole methods and AIR suffer from weak ringing artifacts, in particular at brain interfaces/surface. All partial *k*-space reconstructed images reproduced the essential features of the full *k*-space sampled images both with regard to intensity distributions and evolution over time. The lowest SNR values have been computed with keyhole yet we did not observe a significant difference regarding the SNR values of the three reconstruction methods (Table 2). The quantitative comparison of the experimental full and partial *k*-space sampled data is in line with predictions derived from simulations.

rCTC curves for a representative animal for the full *k*-space and partial (25%) *k*-space reconstructed images are depicted in Fig. 7. The higher sampling rate associated with reduced *k*-space acquisition improves the accuracy of the estimation process. When comparing the profiles to the full *k*-space sampled data, it becomes obvious that AIR and m_keyhole yield superior results to keyhole. In fact, rCTC curves for AIR and m_keyhole data are almost identical. An interesting observation is that keyhole reconstruction largely underestimates CA recirculation in agreements with the results obtained from the simulation studies. The difference performance of the reconstruction algorithms is also reflected by the quantitative perfusion values derived (Table 2). The values of the mean rCBV, MTT and rCBF were computed for the ten rats (five each for full and partial *k*-space sampled data). Perfusion parameters obtained for AIR images deviated −26% for rCBV, 0% for MTT and 26% for rCBF, when compared to the reference values computed for the full *k*-space reconstructed data, which is within one standard

Table 1 Quantitative evaluation of simulation results: Mean values of rCBV, MTT and rCBF have been determined in a region of interest located in the cerebral cortex (a) and in brain striatum (b)

	Full *k*-space	keyhole	m_keyhole	AIR
a				
rCBV	1.19	0.78 (34%)	0.89 (25%)	1.22 (−3%)
MTT	0.62	0.62	0.62	0.62
rCBF	1.92	1.27 (34%)	1.43 (26%)	1.97 (−3%)
SNR	20.86	12.69 (38%)	18.02 (14%)	17.64 (15%)
b				
rCBV	0.66	0.39 (41%)	0.46 (30%)	0.64 (3%)
MTT	0.45	0.19 (58%)	0.34 (24%)	0.35 (22%)
rCBF	1.47	2 (−36%)	1.35 (8%)	1.83 (−24%)
SNR	21.84	20.73 (5%)	20.88 (4%)	32.41 (−48%)

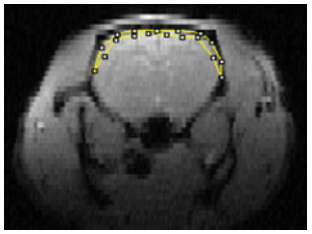

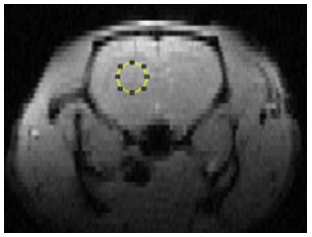

The numbers in the brackets represent the difference in percentage from the full *k*-space reconstructed images. SNR values have been evaluated at the maximum concentration value. 25% of the full *k*-space data were used to compute keyhole, m_keyhole and AIR reconstructed images which are shown in Fig. 3

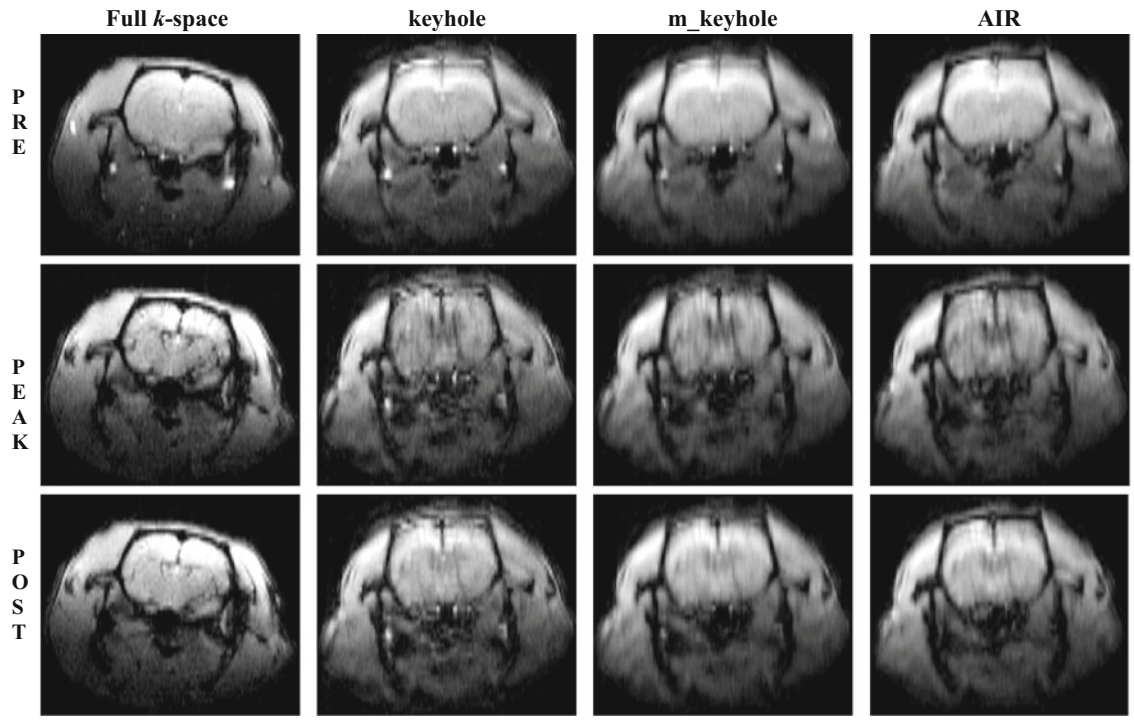

Fig. 6 Axial images of rat brains acquired previous (*top rows*), during (*middle rows*) and after (*bottom rows*) the CA passage. Left column are full *k*-space reconstructed images while the other columns are images reconstructed with keyhole, m_keyhole and AIR reconstruction methods, respectively. Full *k*-space and partial *k*-space data were acquired in two different sets (same animal for reduced acquisition time *k*-space). Only 25% of the full *k*-space data are acquired to perform keyhole and AIR reconstruction

Table 2 Quantitative evaluation: rCBV, MTT and rCBF were estimated for a cortical region of interest

	Full *k*-space	keyhole	m_keyhole	AIR
CBV	1.42 ± 0.36	0.83 ± 0.18 (42%)	1.06 ± 0.19 (25%)	1.05 ± 0.45 (26%)
MTT	0.77 ± 0.04	0.55 ± 0.03 (29%)	0.58 ± 0.03 (25%)	0.57 ± 0.04 (26%)
CBF	1.86 ± 1.17	1.79 ± 0.46 (2%)	1.84 ± 0.50 (1%)	1.86 ± 0.92 (0%)
SNR	15.22 ± 1.82	11.96 ± 4.24 (21.42%)	13.59 ± 2.08 (10.7%)	12.5 ± 2.32 (17.9%)

Values are given as mean ± SEM ($N = 5$ animals) with the numbers in the brackets representing the difference in percent from the full *k*-space reconstructed images. SNR values have been evaluated at the maximum concentration value. Partial *k*-space sampling comprised 25% of the full *k*-space corresponding to an increase in temporal resolution by a factor of 4

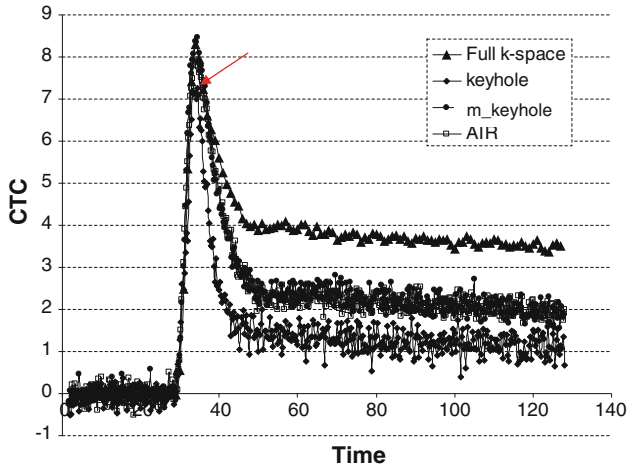

Fig. 7 Quantitative evaluation of perfusion data: Concentration–time curve (CTC) from full and reduced *k*-space (25%) reconstructions. Again the *arrow* indicates the peak of the keyhole CTC curve. Reducing *k*-space coverage increases the number of data points in time domain by a factor of 4

deviation of the reference values. M_keyhole provided similar results while the perfusion estimates for keyhole reconstructed data were significantly lower with deviations of −42% for rCBV, −2% for rCBV and −29% for MTT. One explanation for larger standard deviations in image intensity could be the related to the considered ROI (i.e. tissue with large vessels would be expected to show increased variability).

Discussion

The present work describes the use of the analytic image concept for reconstructing DSC-MRI data. Accelerating data acquisition by reduced *k*-space sampling can be exploited in several ways: (1) the higher sampling rate improves the definition of the rCTC curves and therefore the quality of the perfusion parameters derived. (2) Alternatively, accelerated data acquisition allows coverage of larger tissue volumes using either multislice or 3-dimensional data acquisition strategies.

When comparing AIR to other related reconstruction techniques such as keyhole, it could be shown to produce superior results, in particular the overall image intensity is better reproduced, which is critical for deriving perfusion values. This has been concluded both from simulated data and from experimental results obtained with an acceleration factor of 4 (25% of *k*-space sampled). Comparable results have been achieved using a modified keyhole approach (m_keyhole) with the weighting of the low spatial frequencies increased by a factor of 2.

In AIR, only one half of the baseline high spatial frequencies acquired prior to the DSC-MRI series are used for reconstruction: AIR uses the positive frequencies associated with the static information in the image and exploits the pseudo-Hermitian symmetry of the *k*-space to recover the missing *k*-space data during the reconstruction process. This procedure avoids some artifacts as e.g. those introduced by keyhole reconstruction (see arrows in Fig. 3). It further more leads to an improvement of SNR values in the reconstructed images. Despite obvious similarities, keyhole and AIR use two different reconstruction strategies. While keyhole fills in missing high-frequency data simply with those from the baseline data set(s), AIR recovers the missing data using the analytic image concept, which exploits redundancies in *k*-space data. A major aspect of AIR is the increased weight of the low spatial frequencies during the reconstruction process leading to a better recovery of image contrast.

Since CA passage through the brain vasculature corresponds to an incoherent, diffusion like propagation, the high spatial frequency components will not be identical to those of the baseline image; as a consequence, there will be incoherence in the assembled raw data (discontinuity in intensity and phase), which would lead to image artifacts. It has been reported that keyhole imaging degrades the resolution of the dynamic image change in presence of higher spatial frequency content [5]. This behavior, which becomes obvious before and after the first pass of the CA, explains the low signal amplitude observed during CA recirculation and potentially also the occurrence of discrete image artifacts (Fig. 5). The low pass filter inherently used in AIR increases the most important part of the information related

to the object (low spatial frequencies), so the intensity contribution of the static part of the data (high spatial frequencies) is lower compared to that of the dynamic part (low spatial frequencies), while in keyhole both contribute equally. The presented modified version of keyhole, m_keyhole, not only improves the reconstruction from a qualitative point of view but also with regard to quantitative intensity values. It is nevertheless worth to pinpoint attention on the fact that the reconstruction quality is related to the quality of the DSC-MRI procedure. In order words, one should care about undesired effects, which can corrupt the quality of the reconstructed image. For example, for T_2^*-weighted DSC-MRI, CA induced decreases of T_1 will affect both the measurement of AIF and of CTC in tissue, although to a lesser extent because of its small contribution from the intravascular compartment. When increasing the temporal resolution of DSC-MRI, one should care about parameters used for optimizing the imaging sequence. Thus, inappropriate values of TR, TE and flip angle may lead to unwanted T_1-weighting [22] or an insufficient SNR. For the current study, this was not an issue as both full and partial *k*-space sampled data sets have been acquired using identical sequence parameters.

In keyhole, the reconstructed images represent the summation of the baseline image with the difference between the images of the dynamic series and the mentioned baseline convolved with the filter function that is associated to the keyhole window. In contrast, AIR uses high frequencies corresponding to the static information of the series once by applying another convolution term associated to the filter function involved for the missing *k*-space data (see Eq. 6). This leads to an improvement in SNR considering the overall image, which may come at a certain cost. The increase in SNR in the reconstructed images may be linked to a loss of spatial resolution as reflected by the AIR DSC-MRI images presented in Figs. 3 and 6. Advantages of AIR are that assumptions about the signal distribution are not required and at the same time, the method does not over-constrain the reconstruction algorithm like in constraint Fourier imaging or some parallel imaging reconstruction approaches. Also, in contrast to the keyhole approach, AIR does not required assumptions, like the right orientation of the phase-encoding direction previously mentioned, to expect useful quantitative results [5].

The ringing artifacts in the reconstructed images (Figs. 3 and 6) are the result of data substitution (discontinuity in phase and intensity) and in the case of AIR to sharp transitions in the *k*-space domain when using a step function as a filter (see Eq. 6). These artifacts can largely be reduced by applying a smoothing filter, which, however, will affect the quantitative perfusion parameters as the signal intensities are modified. Therefore, we refrained from using smoothing filters in this study.

Conclusion

We have investigated the use of the AIR algorithm for DSC-MRI reconstruction in small animal studies. AIR exploits pseudo-Hermitian property of the *k*-space through the analytic image concept in order to improve the reconstruction quality and to allow computation of reasonable perfusion parameters. Using AIR reduces *k*-space signal drifts effects compared to the keyhole approach and allows a better reconstruction of the dynamic stage of the image series thus leading to better dynamic effects analysis. AIR preserves a good reconstruction, both qualitatively and quantitatively, of DSC-MRI while allowing a reduction in the acquisition time by a factor up to 4. An alternative approach to improve quantitative intensity information derived from the keyhole reconstruction is a modified version thereof, m_keyhole, with increased weighting of the low spatial frequencies.

Acknowledgments We sincerely thank Esther Sydekum and Dr. Ivana Kotevic, for animal preparation and monitoring and the Swiss National Science Foundation for funding.

References

1. van Vaals JJ, Brumer ME, Dixon WT, Tuithof HH, Engels H, Nelson RC, Gerety BM, Chezmar JL, den Boer JA (1993) Keyhole: method for accelerating imaging of contrast agent uptake. J Magn Reson Imag 3:671–675
2. Walsh EG, Doyle M, Lawson MA, Blackwell GG, Pohost GM (1995) Multislice first-pass myocardial perfusion imaging on clinical scanner. Magn Reson Med 34:39–47
3. Suga M, Matsuda T, Komori M (1999) Keyhole method for high-speed human cardiac cine MR imaging. J Magn Reson Imag 10:778–783
4. Parrish T, Hu X (1995) Continuous update with random encoding (CURE): a new strategy for dynamic imaging. Magn Reson Med 33:326–336
5. Oesterle C, Strohschein R, Köhler M, Schnell M, Hennig J (2000) Benefits and pitfalls of keyhole imaging, especially in first-pass perfuson studies. J Magn Reson Imag 11:312–323
6. Zaitsev M, Zilles K, Shah NJ (2001) Shared k-space echo-planar imaging with keyhole. Magn Reson Med 45:109–117
7. Doyle M, Walsh EG, Blackwell GG, Pohost GM (1995) Block regional interpolation scheme for k-space (BRISK): a rapid cardiac imaging technique. Magn Reson Med 33:163–170
8. Hu X, Parrish T (1994) Reduction of field of view for dynamic imaging. Magn Reson Med 31:691–694
9. Jones RA, Haraldseth O, Muller TB, Rinck PA, Oksendal AN (1993) K-space substitution: a novel dynamic imaging technique. Magn Reson Med 29:830–834
10. Zaitsev M, Zilles K, Shah NJ (2001) Shared k-space echo-planar imaging with keyhole. Magn Reson Med 45:109–117
11. Korosec FR, Frayne R, Grist TM, Mistretta CA (1996) Time-resolved contrast-enhanced 3D MR angiography. Magn Reson Med 36:345–351
12. Yankam Njiwa J, Zhu YM, Robini M, Magnin I (2007) Magnetic resonance image reconstruction using the notion of analytic image. Nucl Instr Meth Phys Res A 1(2):73–76

13. Noll DC, Nishimura DG, Macovski A (1991) Homodyne detection in magnetic resonance imaging. IEEE Trans Med Imag 10:154–163
14. McGibney G, Smith MR, Nicholas ST, Crawley A (1993) Quantitative evaluation of several partial-Fourier reconstruction algorithms used in MRI. Magn Reson Med 30:51–59
15. Yankam Njiwa J, Hiba B, Zhu YM (2007) Cardiac cine MR reconstruction from partial k-space. In: IEEE proceeding
16. Liu HL, Pu Y, Liu Y, Nickerson L, Andrews T, Fox PT, Gao JH (1999) Cerebral blood flow measurement by dynamic contrast MRI using singular value decomposition with an adaptive threshold. Magn Reson Med 42:167–172
17. Yeh MY, Lee TH, Yang ST, Kuo HH, Chyi TK, Liu HL (2009) Automated detection of arterial input function in DSC perfusion MRI in a stroke rat model. J Instrum 18:14–23
18. Newman GC, Hospod FE, Fain SB, Cook TD (2006) Optimizing dynamic T2* MR imaging for measurement of cerebral blood flow using infusions for cerebral blood volume. AJNR Am J Neuroradiol 26:1239–1240
19. Ostergaard L, Weisskoff RM, Chesler DA, Gyldensted C, Rosen BR (1996) High resolution measurement of cerebral blood flow using intravascular tracer bolus passages. Part I Math Approach Stat Anal Magn Reson Med 36:715–725
20. Rempp KA, Brix G, Wenz F, Becker CR, Gückel F, Lorenz WJ (1994) Quantification of regional cerebral blood flow and volume with dynamic susceptibility contrast-enhanced MR imaging. Radiology 193:637–641
21. Meier P, Zierler KL (1954) On the theory of the indicator-dilution method for measurement of blood flow and volume. J Appl Physiol 6:731–744
22. Calamante F, Vonken EJ, Osch MJ (2007) Contrast agent concentration measurements affecting quantification of bolus-tracking perfusion MRI. Magn Reson Med 58:544–553